Cooperative Swinging of Complex Pendulum-Like Objects: Experimental Evaluation

Philine Donner and Martin Buss

***Abstract*—Cooperative dynamic object manipulation increases the manipulation repertoire of multiagent teams. As a first step toward cooperative dynamic object manipulation, we present an energy-based controller for cooperative swinging of two-agent pendulum-like objects. Projection of the complex underactuated mechanism onto an abstract cart–pendulum allows us to separate desired and undesired oscillations. The desired oscillation is excited up to a desired energy level, while an undesired oscillation can be actively damped. Communication between the agents is restricted to force feedback. The controller can render leader and follower agents. The follower actively assists the swinging task by imitating the leader's energy flow. Real-world experiments with a robot and a human swinging complex pendulum-like objects are presented. The experimental results indicate that no simultaneous damping of the undesired oscillation is needed, also because it disturbs the human partner. A successful contribution of the robotic follower to the swing-up effort in interaction with a human leader supports the proposed control approach.**

***Index Terms*—Cooperative manipulators, dynamic manipulation, force and tactile sensing, physical human–robot interaction, suspended loads.**

I. Introduction

This study is motivated by the belief that cooperative dynamic manipulation extends the manipulation capabilities of multiagent teams. Cooperative manipulation extends the range of objects that can be manipulated to higher loads and bulky objects. Examples are carrying suspended loads by aerial load transportation systems to areas that are difficult to access [1], as well as moving bulky furniture in home environments. Dynamic manipulation comprises manipulation strategies that make use of the object dynamics [2] with the advantage of an extended "repertoire of actions" available to manipulators: Larger objects can be handled more quickly by simpler end effectors and outside the workspace of the manipulator [3]. Cooperative dynamic manipulation brings the advantages of cooperative and dynamic manipulation together. As a motivational example for cooperative human–robot object swinging, imagine the joint manipulation of a sports mat, as presented in Fig. 1. Through synchronous incremental energy injection, the bulky flexible sports mat is brought to a higher elevation, at which it can be released to be placed onto a stack of mattresses. Consequently, the combination of more than one agent and dynamic swing motion allows the manipulation of large and heavy loads, which might be infeasible to be handled by a single agent or through pure translational motion. Moreover, a flight phase following the swing-up phase increases the reachable workspace.

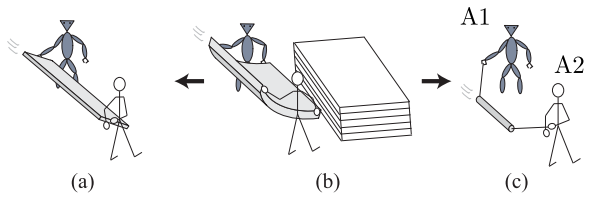

Fig. 1. Classification of (a) flexible object swinging as a combination of (b) rigid object swinging and (c) pendulum swinging.

Swinging of flexible objects [see Fig. 1(b)] can be interpreted as a mixture of two extremes: swinging of rigid objects, in which the manipulators/arms of the agents together with the rigid object form an oscillating entity [see Fig. 1(a)], and swinging of pendulum-like objects, which can oscillate themselves [see Fig. 1(c)]. The focus of this paper is on two-agent cooperative swinging of pendulum-like objects.[1] Pendulum-like objects like the one in Fig. 1(c) are also referred to as slung loads or suspended loads in the literature. The agents can form human–robot or also purely robotic teams. We assume that communication between the agents is restricted to the forces exchanged via the physical coupling through the manipulated object. The control goal is to reach a desired level of energy stored in the object oscillation. The desired energy level is equivalent to a desired maximum object height or maximum deflection angle at the turning points and represents a periodic orbit in the state space of the pendulum-like object. Disturbance oscillations in additional degrees of freedom (DoFs) of the underactuated mechanism are to be damped. The controller can render a robotic leader and follower. While the leader knows the desired energy level, the follower needs to infer the partner's intention from the interaction with the object in order to actively assist. In the following, we present the literature that is relevant to the different aspects of our approach.

A. Manipulation of Suspended Loads

Applications for the manipulation of suspended loads are found in aerial vehicles or crane systems. The highly nonlin-

Manuscript received January 27, 2016; accepted April 23, 2016. Date of publication June 3, 2016; date of current version June 3, 2016. This paper was recommended for publication by Associate Editor P. R. Giordano and Editor T. Murphey upon evaluation of the reviewers' comments. This work was supported in part by the European Research Council under the European Union's Seventh Framework Program (FP/2007-2013)/ERC Grant 267877 and in part by Technical University of Munich—Institute for Advanced Study (www.tum-ias.de), funded by the German Excellence Initiative.

The authors are with the Chair of Automatic Control Engineering and the TUM Institute for Advanced Study, Technical University of Munich, 85748, Garching, Germany (e-mail: philine.donner@tum.de; mb@tum.de).

This paper has supplementary downloadable material available at http://ieeexplore.ieee.org, provided by the author. The material consists of a video, viewable with VLC Media Player (2.1.4 Rincewind), showing in detail the four experiments that are analyzed in the paper, including the following evolution of energies and energy flows over time: 1) Robot leader fixed end a) with active disturbance damping and b) without active disturbance damping and 2) Robot follower human leader: a) with active disturbance damping and b) without active disturbance damping. Contact philine.donner@tum.de for further questions about this work.

Color versions of one or more of the figures in this paper are available online at http://ieeexplore.ieee.org.

Digital Object Identifier 10.1109/TRO.2016.2560898

[1] Swinging of rigid objects is treated in [4].

ear dynamics of aerial vehicles makes their control challenging. Therefore, and for reasons of safety, the focus has been on damping of undesired oscillations. Most approaches look into object manipulation via a single suspension. The cascaded control approach in [1] can control two or more small helicopters to jointly carry a suspended load. Zemrovski, Starr, Wood, and Lumia use dynamic programming to perform fast swing-free load transport by two independent robotic manipulators [5].

In contrast with the aforementioned works, we aim at making use of oscillations instead of only damping them. As a consequence, the manipulation repertoire is increased, energy can be injected swing by swing, and the manipulator workspace can be extended, e.g., a load transported by a quadrotor could reach below overhangs. Despite these advantages, only a few works exist that exceed the control benchmark problem of inverted pendulum swing-up. Recently, de Crousdaz, Farshidian, Neunert, and Buchli showed how controlled energy injection into a slung load transported by a quadrotor allows the system to fly through a window, which is too small to be passed with the load hanging down [6]. Parametric excitation is used to control single-cable-suspended mechanisms in [3], [7], and [8] and double-cable-suspended mechanisms in [9] and [10]. The suspended objects in [5] and [9] are similar to the object under consideration in this paper [see Fig. 1(c)]. However, the approaches in the literature either only damp oscillations [5] or use one centralized controller for both control inputs [9].

B. Dynamic Manipulation in Physical Human–Robot Interaction

Physical human–robot interaction addresses tasks during which a human and a robot are in contact, directly or through an object. Within cooperative object manipulation, the focus has been on cooperative transport of rigid objects. In contrast with such kinematic manipulation [2], dynamic manipulation requires to take the object dynamics into account in order to achieve a certain object trajectory through appropriate end effector motion. Only limited work exists on human–robot cooperative dynamic object manipulation. Rope turning of a human and a robot is investigated in [11] and [12]. However, the robot controllers are only able to sustain a stable rope turning motion, which was established beforehand by the human.

Research in the area of human–robot cooperative kinematic object manipulation has seen great interest. Starting from passive assistants [13], the goal shifted toward robotic partners that actively contribute to the task goal [14]. In this study, we restrict the robotic agents to haptic feedback only, meaning that they have to infer the state of the object as well as the intention of the partner through the measured interaction forces only in order to actively contribute to the task. Motivated by the finding that humans switch roles during haptic interaction tasks [15], Evrard and Kheddar introduce a homotopy switching model to blend between leader and follower behaviors [16]. Mörtl *et al.* define effort roles, which specify how the task effort is split among the agents in the redundant task directions [17]. For many kinematic manipulation tasks, the leader's intention is reflected in a planned trajectory. In contrast, for the swinging task, the leader's intention is reflected in a desired object energy that is a stable periodic orbit. An important difference of the dynamic compared with the kinematic manipulation task is the loose coupling through the pendulum-like object. Consequently, the direct mapping of measured interaction force to leader intention as done in many kinematic manipulation tasks (e.g., see [17] and [18]) does not apply. We propose a follower that compensates for a lack of knowledge regarding the desired periodic orbit, by monitoring and imitating the energy flow produced by the leader.

C. Simple Pendulum-Based Energy Control

Simple pendulum approximations are frequently used to model and control complex underactuated mechanisms. Examples are biped walking [19] and brachiation [20]. The goal of the cooperative swinging task discussed in this paper is to achieve a simple pendulum-like oscillation of the complex underactuated mechanism. We use an observer with simple pendulum dynamics to separate desired and undesired oscillations. What remains is the task to control the energy content of the individual oscillations to the desired periodic orbit. The swing-up of pendulums and their subsequent stabilization in the unstable equilibrium is a common application to test linear and nonlinear control concepts, e.g., [21] and [22]. We build our energy control on the cart–pendulum swing-up controller by Yoshida [23].

D. Contribution and Outline

In our previous works, we introduced the task of cooperative pendulum swinging, starting with a v-shaped pointmass pendulum in [24], which was extended to the more complex trapezoidal pendulum in Fig. 1(c) in [25]. Experiments in both works were limited to virtual reality experiments, which allowed for human interaction but used an ideal simulated object and robotic partner. In this study, we evaluate our control approach in experiments with a robotic manipulator and real pendulum-like objects.

The remainder of this paper is organized as follows. In Section II we formally state our problem. The main ideas of the control approach and its implementation are presented in Section III. Experiments with a robotic manipulator and real pendulum-like objects follow in Section IV. We draw our conclusion in Section V.

II. Problem Formulation for Cooperative Swinging

This study presents a controller design for cooperative dynamic manipulation of a pendulum-like object through two agents, A1 and A2 [see Fig. 1(c)]. In this section, we introduce the complex pendulum-like object used throughout this paper and formally state the problem.

A. T-Pendulum

We use a dual-lift system with a cylindrical object as an example for a complex pendulum-like object (see Fig. 2 with details in the caption). We refer to it as a t-pendulum due to its trapezoidal shape. Under the assumption of point-mass handles,

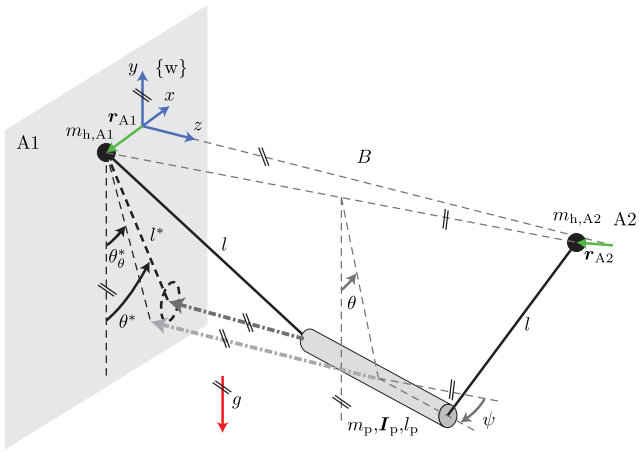

Fig. 2. T-pendulum: cylindrical pendulum object of mass m_{p}, length l_{p}, and inertia I_{p} suspended from two handles of mass $m_{\mathrm{h},Ai}$ located at r_{Ai} with $i = 1, 2$ through massless ropes of length l. The pendulum is under the influence of gravity g. The initial distance between the two agents is B. The location r_{A1} is defined with respect to the world fixed coordinate system $\{\mathrm{w}\}$. The location r_{A2} is defined with respect to the fixed point ${}^{\mathrm{w}}p = [0\ 0\ B]^T$ in $\{\mathrm{w}\}$. Pairs of parallel lines at the same angle indicate parallelity.

the t-pendulum has 10 DoFs. We further neglect rotations of the cylindrical object around its center line and oscillations in the t-pendulum plane (around the horizontal axis perpendicular to the connection line between the interaction partners).[2] This leaves us with eight generalized coordinates that fully describe the configuration of the t-pendulum: the 3-D positions of the two handles $\boldsymbol{r}_{Ai}$ and the two angles θ and ψ, which we refer to as oscillation DoFs throughout this paper. The desired oscillation DoF θ describes oscillations of the object around the connection line between the interaction partners (angle between the plane defined by $\boldsymbol{r}_{Ai}$ and the y-axis and the plane defined by $\boldsymbol{r}_{Ai}$ and the center of mass of the object). The disturbance oscillation DoF ψ describes oscillations of the object around the y-axis (angle between the plane defined by $\boldsymbol{r}_{Ai}$ and the y-axis and the plane along the object center line parallel to the y-axis). The state vector results in $\boldsymbol{x} = \left[\theta\ \psi\ \dot{\theta}\ \dot{\psi}\ \boldsymbol{r}_{\mathrm{A1}}\ \dot{\boldsymbol{r}}_{\mathrm{A1}}\ \boldsymbol{r}_{\mathrm{A2}}\ \dot{\boldsymbol{r}}_{\mathrm{A2}}\right]^T$.

The control approach is based on a projection of the complex t-pendulum onto a cart–pendulum of length l^* and deflection angle θ^*. The projection is carried out along the z-axis as illustrated by the dark gray dashed–dotted arrow in Fig 2. The projected deflection angle θ^* in the xy plane is caused by a superposition of the θ-oscillation and the ψ-oscillation

$$\theta^* = \theta^*_\theta + \theta^*_\psi \tag{1}$$

where θ^*_θ is the angle that results from a projection of the center of mass of the t-pendulum onto the xy plane (light gray dashed–dotted arrow in Fig 2). We use θ^*_ψ for the difference $\theta^* - \theta^*_\theta$, as its main origin are ψ-oscillations. For a synchronous motion of the agents, zero disturbance oscillation $\psi \approx 0$ is to be expected, leading to $\theta = \theta^* = \theta^*_\theta$. Independent motion of the agents, however, causes the initial distance B between the agents to alter and the projected length l^* to change. The presented control approach requires knowledge of l^*. We use $l^*(\boldsymbol{x} = \boldsymbol{0})$ for our controllers, which leaves us with a relatively small mistake as $B \gg \left\| \boldsymbol{r}_{Ai} \right\|_2$ in our setup. Furthermore, nonzero disturbance oscillation $\psi \neq 0$ has the effect that $\theta^*_\psi \neq 0$ and, consequently, $\theta^*_\theta \neq \theta^*$. For cylinder length $l_{\mathrm{p}} \to 0$, the t-pendulum simplifies to a v-shaped point mass pendulum without disturbance oscillation ψ, which we refer to as v-pendulum [24].

B. Problem Statement

The objective is to control the pendulum-like object to reach the desired periodic orbit

$$\mathcal{O}(\boldsymbol{x}) : \begin{cases} E_\theta = E^{\mathrm{d}}_\theta = m_{\mathrm{p}} g h^{\mathrm{d}}_E = m_{\mathrm{p}} g l^* (1 - \cos(\theta^{\mathrm{d}}_E)) \\ E_\psi = E^{\mathrm{d}}_\psi = 0 \\ \boldsymbol{r}_{Ai} = \dot{\boldsymbol{r}}_{Ai} = \boldsymbol{0} \quad \text{with} \quad i = 1, 2 \end{cases} \tag{2}$$

where E_θ and E_ψ are the energies contained in the θ- and ψ-oscillations and the superscript d signifies their desired values. Thus, the desired oscillation DoF θ is to be excited such that the oscillation reaches the energy E^{d}_θ, which is equivalent to a maximum deflection angle θ^{d}_E or desired object height h^{d}_E. The energy contained in the θ-oscillation is computed by

$$E_\theta = \frac{1}{2} m_{\mathrm{p}} l^{*2} \dot{\theta}^2 + m_{\mathrm{p}} g l^* (1 - \cos(\theta)). \tag{3}$$

The object state $\boldsymbol{x}$ can be influenced through acceleration of the agents' interaction points $\boldsymbol{u} = \ddot{\boldsymbol{r}}_{\mathrm{A1}}$ and $\boldsymbol{z} = \ddot{\boldsymbol{r}}_{\mathrm{A2}}$. Although we assume cooperative interaction, only the behavior of agent A1 can be directly controlled. Consequently, the input of agent A2 is defined as disturbance $\boldsymbol{z}$. We assume that the sensor feedback of agent A1 is limited to the forces applied at its own end effector $\boldsymbol{y}_{\mathrm{m}} = \boldsymbol{F}_{\mathrm{A1}}$. Although A2 might move in 3-D, we limit the motion of agent A1 to the x-direction for simplicity,[3] i.e., $\boldsymbol{u} = \left[u\ 0\ 0\right]^T = \left[\ddot{r}_{\mathrm{A1}}\ 0\ 0\right]^T$.

We distinguish between a leader $\mathrm{A1} = \mathcal{L}$ and a follower agent $\mathrm{A1} = \mathcal{F}$. A leader $\mathcal{L}$ knows the desired periodic orbit $\mathcal{O}(\boldsymbol{x})$ including the desired energy levels E^{d}_θ and E^{d}_ψ. Thus, we are looking for a control law

$$u_{\mathcal{L}} = \ddot{r}_{\mathcal{L}} = f(\boldsymbol{y}_{\mathrm{m}} = \boldsymbol{F}_{\mathcal{L}})$$
$$\text{such that} \quad \left| E^{\mathrm{d}}_j - E_j(t > T_{\mathrm{s}}) \right| \leq \epsilon_j \ \text{ with } \ j = \theta, \psi$$
$$\text{for} \quad 0 < T_{\mathrm{s}} < \infty \tag{4}$$

with T_{s} being the system settling time. Consequently, we require the energy errors $\Delta E_j = E^{\mathrm{d}}_j - E_j$ to stay within the ranges ϵ_j the latest after $t = T_{\mathrm{s}}$.

A follower $\mathcal{F}$ has partial knowledge about the desired periodic orbit $\mathcal{O}(\boldsymbol{x})$, i.e., the follower knows which oscillation DoFs to excite and which ones to damp, but not the value of E^{d}_θ. Thus, a follower needs to infer the partner's intention—increase, hold,

[2]The in-plane oscillation was shown to play a minor role for robot motion along the x-axis and natural human motion. Therefore, we neglect this oscillation in the following. However, essentially the same controller can be applied along the z-direction to damp these disturbance oscillations (see videos [26]).

[3]One-dimensional motion is sufficient and does not restrict a human partner's 3-D motion due to the loose coupling of the agents through the pendulum-like object. See the video in the multimedia material.

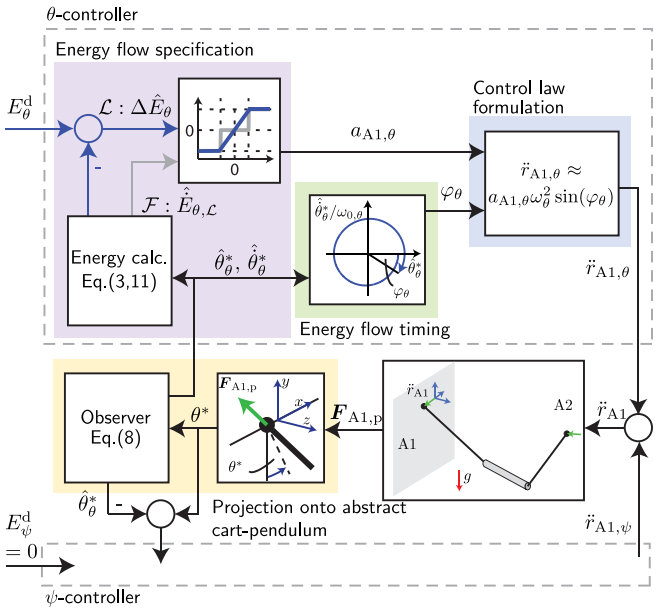

Fig. 3. Block diagram of the energy-based swing-up controller.

or decrease the current system energy E_θ—to actively contribute to the task goal. The follower can achieve this by monitoring and imitating the leader's energy flow $\dot{E}_{\mathcal{L},\theta}$. We define the desired follower behavior as

$$u_\mathcal{F} = \ddot{r}_\mathcal{F} = f(\boldsymbol{y}_\mathrm{m} = \boldsymbol{F}_\mathcal{F}) \quad \text{such that}$$
$$\begin{cases} \dot{E}_{\mathcal{F},\theta} > 0, & \text{if} \quad \dot{E}_{\mathcal{L},\theta} > \delta_{\mathcal{F},\theta} \\ \dot{E}_{\mathcal{F},\theta} = 0, & \text{if} \quad -\delta_{\mathcal{F},\theta} \leq \dot{E}_{\mathcal{L},\theta} \leq \delta_{\mathcal{F},\theta} \\ \dot{E}_{\mathcal{F},\theta} < 0, & \text{if} \quad \dot{E}_{\mathcal{L},\theta} < -\delta_{\mathcal{F},\theta} \end{cases} \tag{5}$$

with $\delta_{\mathcal{F},\theta} > 0$ being a threshold[4] and $\dot{E}_{\mathcal{F},\theta}$ being the energy flow to the oscillation DoF θ produced by the follower. The ψ-oscillation is known to the follower as being undesired. Thus, the follower behaves as a leader with respect to the ψ-oscillation ($E^\mathrm{d}_\psi = 0$).

III. Control Approach

The main ideas of the control approach presented are: 1) to extract the desired and the undesired oscillation DoFs by projecting the complex pendulum-like object onto an abstract cart–pendulum and 2) to apply an energy-based controller to the extracted oscillation to reach the desired periodic orbit $\mathcal{O}(\boldsymbol{x})$.

Fig. 3 shows the block diagram of the control structure with details on the control of the desired θ-oscillation. The control of the ψ-oscillation is structurally similar. Differences are highlighted in Section III-C. In this section, we first introduce the abstract cart–pendulum, followed by an overview of our control method and implementation based on Fig. 3. For details, the reader is referred to our previous work [25].

[4]The threshold δ_i, θ can be adjusted such that the follower does not react to minor energy flow, e.g., that caused by friction.

A. Projection onto the Abstract Cart–Pendulum

For synchronous motion of the agents along the x-axis $\ddot{\boldsymbol{r}}_{\mathrm{A}i} = [\ddot{r}_{\mathrm{A}i}\ 0\ 0]^T$, the disturbance angle is zero $\psi = 0$ and the complex t-pendulum approximately behaves as a cart–pendulum with two-sided actuation

$$\ddot{\theta} = -\frac{g}{l^*}\sin(\theta) - \frac{1}{l^*}\cos(\theta)\frac{\ddot{r}_{\mathrm{A}1} + \ddot{r}_{\mathrm{A}2}}{2}. \tag{6}$$

We call this system an *abstract cart–pendulum*. Cart–pendulum signifies a massless pole of length l^* connecting the point mass m_p and the cart-actuated pivot point. We use the term *abstract* to underline the simplification we make by reducing the influence of the two agents to additive acceleration inputs $\ddot{r}_{\mathrm{A}1}$ and $\ddot{r}_{\mathrm{A}2}$ along the x-axis.

We extract estimates of the desired θ-oscillation in two steps. In a first step, we map the measured forces $\boldsymbol{F}_{\mathrm{A}1}$ to the projected deflection angle θ^* (see Fig. 2) as

$$\theta^* = \arctan\left(\frac{-F_{\mathrm{A}1,\mathrm{p},x}}{F_{\mathrm{A}1,\mathrm{p},y}}\right). \tag{7}$$

The force $\boldsymbol{F}_{\mathrm{A}1,\mathrm{p}} = [F_{\mathrm{A}1,\mathrm{p},x} \quad F_{\mathrm{A}1,\mathrm{p},y} \quad F_{\mathrm{A}1,\mathrm{p},z}]^T$ is the force exerted on the pendulum through agent A1 and is obtained from the measurable end effector force $\boldsymbol{F}_{\mathrm{A}1}$ by dynamically compensating for the force caused by the handle mass $m_{\mathrm{h},\mathrm{A}1}$: $\boldsymbol{F}_{\mathrm{A}1,\mathrm{p}} = \boldsymbol{F}_{\mathrm{A}1} - m_{\mathrm{h},\mathrm{A}1}[\ddot{r}_{\mathrm{A}1} \quad -g \quad 0]^T$.

In a second step, a nonlinear observer extracts estimates $\hat{\theta}^*_\theta \approx \theta^*_\theta$ and $\dot{\hat{\theta}}^*_\theta \approx \dot{\theta}^*_\theta$, which represent the part of the projected deflection angle θ^* belonging to the θ-oscillation in (1) as

$$\dot{\hat{\boldsymbol{\theta}}}^*_\theta = \begin{bmatrix} \dot{\hat{\theta}}^*_\theta \\ -\frac{g}{l^*}\sin(\hat{\theta}^*_\theta) \end{bmatrix} + \boldsymbol{L}_\theta(\theta^* - y), \quad y = \begin{bmatrix} 1 & 0 \end{bmatrix}\hat{\boldsymbol{\theta}}^*_\theta \tag{8}$$

with state vector $\hat{\boldsymbol{\theta}}^*_\theta = [\hat{\theta}^*_\theta \quad \dot{\hat{\theta}}^*_\theta]^T$. The observer represents the abstract cart–pendulum dynamics (6) without inputs. The term $\boldsymbol{L}_\theta(\theta^* - y)$ couples the observer to the t-pendulum. We summarize these two steps as a projection onto the abstract cart–pendulum (see the yellow background in Fig. 3).

We are aware that the dynamics of the v-pendulum (Fig. 2 with a point mass $l_\mathrm{p} \to 0$) and two agents that both only move in the x-direction is already a lot more complex than (6), as it also depends on the agents' relative position $r_{\mathrm{A}1} - r_{\mathrm{A}2}$ and velocity $\dot{r}_{\mathrm{A}1} - \dot{r}_{\mathrm{A}2}$. In this paper, we refrain from deriving the lengthy differential equations of the v- and t-pendulum.[5] Instead, we show that through the projection of the complex pendulums onto the abstract cart–pendulum, we are able to separate the oscillation DoFs such that we can control the oscillation DoFs in a desired manner and design an actively contributing follower. Consequently, we do not try to capture the complex system dynamics with (6), but we extract the desired oscillation by making use of the fact that the desired oscillation behaves as (6).

[5]See, e.g., [27] for slung-load systems.

B. Energy Control of θ-Oscillation

The idea of the swing-up controller proposed by Yoshida [23] is captured in the following approximate control law:

$$\ddot{r}_{\mathrm{A}1,\theta} \approx a_{\mathrm{A}1,\theta}\ \omega_\theta^2 \sin(\varphi_\theta) \tag{9}$$

with ω_θ being the natural frequency of the θ-oscillation. The amplitude factor $a_{\mathrm{A}1,\theta}$ specifies the direction and amount of energy flow induced by agent A1. A well-timed energy injection is achieved through the phase angle φ_θ.

1) Energy Flow Timing φ_θ: A simple pendulum is a highly nonlinear system with energy-dependent natural frequency $\omega_\theta(E_\theta)$ and can, therefore, not be excited to high energy levels with a sinousoidal input of constant frequency. Calculation of the phase angle

$$\varphi_\theta = \mathrm{atan2}\left(-\frac{\dot{\hat{\theta}}^*_\theta}{\omega_{0,\theta}}, \hat{\theta}^*_\theta\right) \tag{10}$$

with the observer states $\hat{\boldsymbol{\theta}}^*_\theta$ and the small-angle approximation of the natural frequency $\omega_{0,\theta} = \sqrt{\frac{g}{l^*}}$ for normalization allows us to excite the θ-oscillation at its natural frequency up to high energy levels.

2) Energy Flow Specification $a_{\mathrm{A}1}$: The time derivative of (3) with (7) results in the energy flow induced by one agent

$$\dot{E}_{\mathrm{A}i,\theta} = -m_\mathrm{p} l^* \dot{\theta} \cos(\theta) \frac{\ddot{r}_{\mathrm{A}i}}{2}. \tag{11}$$

In [25], we show that for $a_{\mathrm{A}i} > 0$ and our region of interest,[6] $-\frac{\pi}{2} < \theta < \frac{\pi}{2}$, the energy flow $\dot{E}_{\mathrm{A}i,\theta} \geq 0$.

For the leader $\mathcal{L}$, we apply a saturated linear mapping from energy error $\Delta\hat{E}_\theta = E^\mathrm{d}_\theta - \hat{E}_\theta$ to amplitude factor $a_{\mathcal{L},\theta}$

$$a_{\mathcal{L},\theta} = \begin{cases} \bar{a}_{\mathcal{L},\theta}\ \mathrm{sgn}(\Delta\hat{E}_\theta), & \text{if} \quad |\Delta\hat{E}_\theta| \geq \delta_{\mathcal{L},\theta} \\ \dfrac{\bar{a}_{\mathcal{L},\theta}}{\delta_{\mathcal{L},\theta}} \Delta\hat{E}_\theta, & \text{else} \end{cases} \tag{12}$$

with $\frac{\bar{a}_{\mathcal{L},\theta}}{\delta_{\mathcal{L},\theta}}$ being the slope of the linear mapping with maximum amplitude factors $\pm\bar{a}_{\mathcal{L},\theta}$, which are approximately equal to the maximum amplitude of the resultant robot motion. The estimate of the energy contained in the θ-oscillation $\hat{E}_\theta$ is calculated based on the observer states $\hat{\boldsymbol{\theta}}^*_\theta$ and (3).

For the follower $\mathcal{F}$, a mapping from estimated leader energy flow $\hat{\dot{E}}_{\mathcal{L},\theta}$ to three discrete amplitude factors is applied as

$$a_\mathrm{dis} = \begin{cases} \bar{a}_{\mathcal{F},\theta}, & \text{if} \quad \hat{\dot{E}}_{\mathcal{L},\theta} \geq \delta_{\mathrm{u},\mathcal{F},\theta} \\ 0, & \text{if} \quad \delta_{\mathrm{u},\mathcal{F},\theta} > \hat{\dot{E}}_{\mathcal{L},\theta} > \delta_{\mathrm{l},\mathcal{F},\theta} \\ -\bar{a}_{\mathcal{F},\theta}, & \text{if} \quad \hat{\dot{E}}_{\mathcal{L},\theta} \leq \delta_{\mathrm{l},\mathcal{F},\theta}. \end{cases} \tag{13}$$

Instead of the linear connection between the two maximum values $\pm\bar{a}_{\mathcal{L},\theta}$ in the case of the leader (12), we define a neutral zone for the follower for estimated energy flows within the limits[7] $]\delta_{\mathrm{l},\mathcal{F},\theta}, \delta_{\mathrm{u},\mathcal{F},\theta}[$. Ramps

$$\dot{a}_{\mathcal{F},\theta} = \tau_\mathcal{F}\ \mathrm{sgn}(a_\mathrm{dis} - a_{\mathcal{F},\theta}) \tag{14}$$

with inverse blending time constant $\tau_\mathcal{F}$ [17] prevent discontinuities in the end effector acceleration $\ddot{r}_{\mathcal{F},\theta}$.

Computation of the leader–induced energy flow estimate $\hat{\dot{E}}_{\mathcal{L},\theta}$ requires filtering. We use a second-order low-pass filter

$$G_\mathrm{lp}(s, D_\mathrm{lp}, T_\mathrm{lp}) = \frac{1}{T^2_\mathrm{lp} s^2 + 2 D_\mathrm{lp} T_\mathrm{lp} s + 1} \tag{15}$$

with damping D_lp and time constant T_lp. Under the assumption of a lossless t-pendulum, the energy flow balance results in the estimate of the leader energy flow

$$\hat{\dot{E}}_{\mathcal{L},\theta} = \hat{\dot{E}}_\theta - \hat{\dot{E}}_{\mathcal{F},\theta} = s G_\mathcal{F}(s) \hat{E}_\theta(s) - G_\mathcal{F}(s) \dot{E}_{\mathcal{F},\theta}(s) \tag{16}$$

with $G_\mathcal{F}(s) = G_\mathrm{lp}(s, D_\mathrm{lp} = 1, T_\mathrm{lp} = T_\mathcal{F})$ of (16) and $\hat{E}_\theta$ and $\dot{E}_{\mathcal{F},\theta}$ according to (3) and (12) based on the observer states $\hat{\boldsymbol{\theta}}^*_\theta$, respectively.

3) Control Law Formulation: As suggested in [23], we do not directly command the acceleration (9), but apply the low-pass filter $G_\theta(s) = G_\mathrm{lp}(s, D_\mathrm{lp} = \zeta, T_\mathrm{lp} = \frac{c_0}{\omega_{0,\theta}})$ of (15) and make use of the sinusoidal shape of (9) to compensate for amplitude and phase shift of the filter.

C. Damping of Undesired ψ-Oscillation

This section explains how to actively damp the undesired ψ-oscillation of a t-pendulum with an approach similar to the control of the θ-oscillation. Again, we choose the approximate control

$$\ddot{r}_{\mathrm{A}1,\psi} \approx a_{\mathrm{A}1,\psi}\ \omega^2_\psi \sin(\varphi_\psi). \tag{17}$$

1) Extraction of ψ-Oscillation: In an ideal simulation environment, the ψ-oscillation can be efficiently extracted by the simple subtraction $\hat{\boldsymbol{\theta}}^*_\psi = \hat{\boldsymbol{\theta}}^* - \hat{\boldsymbol{\theta}}^*_\theta$ according to (1). However, noise in the force measurements leads to a highly distorted angular velocity $\dot{\theta}^*$ when being calculated by first-order numerical differentiation from θ^*. In order to extract smooth states $\hat{\boldsymbol{\theta}}^*_\psi = [\hat{\theta}^*_\psi \quad \dot{\hat{\theta}}^*_\psi]^T$, a second nonlinear observer of the same form as (8) is used with coupling term $\boldsymbol{L}_\psi((\theta^* - \hat{\theta}^*_\theta) - \hat{\theta}^*_\psi)$. The projection of the ψ-oscillation cannot be easily related to a simple pendulum oscillation. However, simulations showed a better approximation of the ψ-oscillation using the nonlinear observer model than a harmonic oscillator as a filter. The small-angle approximation of the natural frequency $\hat{\omega}_{0,\psi}$, as needed within the observer model, was found experimentally.

2) Energy Flow Timing φ_ψ: The approximation of the natural frequency $\hat{\omega}_{0,\psi}$ is used together with the estimated state $\hat{\boldsymbol{\theta}}^*_\psi$ to compute the phase angle φ_ψ related to the ψ-oscillation according to (10).

[6] In order to be able to approximate the massless suspension ropes as rigid, we do not consider higher maximum deflection angles than $\theta_E = \frac{\pi}{2}$.

[7] Separate lower $\delta_{\mathrm{l},\mathcal{F},\theta}$ and upper $\delta_{\mathrm{u},\mathcal{F},\theta}$ limits allow us to take into account that friction shifts the leader energy flow estimates toward negative values.

3) Energy Flow Specification $a_{\mathrm{A1},\psi}$: For the follower as well as for the leader, the objective is to regulate the energy contained in the ψ-oscillation to zero $E_\psi^{\mathrm{d}} = 0$ [see (2)]. The leader mapping of the θ-oscillation control (13) is reused with parameters $\delta_{\mathcal{L},\psi}$, $\bar{a}_{\mathcal{L},\psi}$ to compute an amplitude factor $a_{\mathcal{L},\psi}$ based on the pseudoenergy $\hat{E}_\psi$ according to (3) and observer states $\hat{\boldsymbol{\theta}}_\psi^*$. The pseudoenergy $\hat{E}_\psi$ is not a real energy, but allows us to quantify the disturbance oscillation. One drawback of its computation according to (3) is that $\hat{E}_\psi$ is not constant for a pure ψ-oscillation, but oscillates. We reduce these oscillations by applying the filter $G_{E,\psi}(s) = G_{\mathrm{lp}}(s, D_{\mathrm{lp}} = 1, T_{\mathrm{lp}} = T_\psi)$ of (15) to the pseudoenergy $\hat{E}_\psi$.

4) Control Law Formulation: In contrast with the θ-controller, the extracted ψ-oscillation does not only contain higher but also lower frequency components than ω_ψ originating from the θ-oscillation. In order to damp all frequencies other than the one of interest ω_ψ, we apply a bandpass filter $G_\psi(s) = s^2(\frac{c_0}{\hat{\omega}_{0,\psi}})^2 G_{\mathrm{lp}}^2(s, D_{\mathrm{lp}} = \zeta, T_{\mathrm{lp}} = \frac{c_0}{\hat{\omega}_{0,\psi}})$ based on the low-pass filter of (15). Again, we compensate for amplitude and phase shift, as suggested in [23].

We add $\ddot{r}_{\mathrm{A1},\psi}$ to the acceleration computed to control the θ-oscillation to form the final control input

$$\ddot{r}_{\mathrm{A1}} = \ddot{r}_{\mathrm{A1},\theta} + \ddot{r}_{\mathrm{A1},\psi}. \tag{18}$$

IV. Experiments

The controller shows convincing performance in simulation and in virtual reality for the v- and the t-pendulum [24], [25]. However, in these cases, the robot and the object are simulated and thus show ideal behavior. In this section we evaluate the control approach presented in Section III in real-world experiments with and without a human interaction partner. Consequently, the controller is tested under the influence of noise and nonideal object and robot behavior.[8]

A. Experimental Procedure

Experiments under multiple conditions were performed: v- or t-pendulum, with or without ψ-damping in the case of the t-pendulum, interaction with a human or with one side of the object being fixed to the environment and different leader/follower role assignments. The following two pairs of t-pendulum experiments are presented in detail (see the video in the multimedia material).

1) Robot Leader and Fixed End (RL-0): The handle of agent $\mathrm{A2} = 0$ was fixed at distance B with respect to the robot $\mathrm{A1} = \mathrm{R} = \mathcal{L}$. At the start of each trial, the cylindrical pendulum mass was released at a pose with significant disturbance oscillation $\psi(t = 0) > 35°$, while the desired oscillation contained almost no energy $\theta(t = 0) \approx 0°$. The desired energy level was set to $\theta_E^{\mathrm{d}} = 40°$.

2) Robot Follower and Human Leader (RF-HL): The trials started from rest $\theta(t = 0) = \psi(t = 0) \approx 0°$. The human interaction partner (agent $\mathrm{A2} = \mathrm{H} = \mathcal{L}$) was asked to inject energy into the pendulum such that a desired energy level of $\theta_E^{\mathrm{d}} = 40°$ is reached, to track the desired constant energy level and to release the t-pendulum energy again. The desired energy level was displayed to the human in form of horizontal lines to which the t-pendulum had to be aligned to at its turning points (see Fig. 4). The robot supported the human leader as a follower $\mathrm{A1} = \mathrm{R} = \mathcal{F}$.

[8]Due to the highly complex dynamics and the interaction with a human, we are not able to provide theoretical convergence guarantees. A stability proof for the abstract cart–pendulum is given in [26].

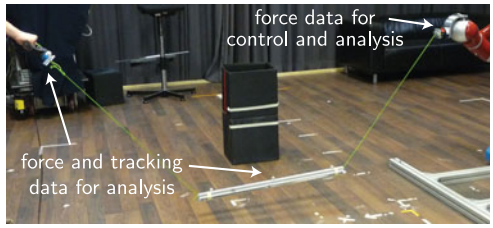

Fig. 4. Experimental setup.

TABLE I
Pendulum and Controller Parameters

m_{p}	l_{p}	d_{p}	l	B	$\omega_{0,\theta}$	m_{h}
1250 g	85 cm	5 cm	96 cm	200 cm	3.57 rad/s	255 g
$\boldsymbol{L}_\theta$, $\boldsymbol{L}_\psi$	$\hat{\omega}_{0,\psi}$	$\delta_{\mathcal{L},\theta}$	$\bar{a}_{\mathcal{L},\theta}$	$\bar{a}_{\mathcal{F},\theta}$	$\delta_{u,\mathcal{F},\theta}$	$\delta_{l,\mathcal{F},\theta}$
$[\omega_{0,\theta}\ 0]^T$	$2\omega_{0,\theta}$	0.5 J	4 cm	4 cm	0.12 W	0.18 W
$\tau_{\mathcal{F}}$	$T_{\mathcal{F}}$	c_0	ζ	$\delta_{\mathcal{L},\psi}$	$\bar{a}_{\mathcal{L},\psi}$	T_ψ
$10\ 1/\mathrm{s}$	$\frac{4.5}{\omega_{0,\theta}}$	0.9	1.2	0.2 J	3 cm	$\frac{1.5}{\omega_{0,\theta}}$

B. Experimental Setup

1) Hardware Setup: Fig. 4 shows the experimental setup. A *KUKA LWR 4+* under impedance control on joint level (joint stiffness 1500 N·m/rad and damping 0.7 N·m·s/rad) served as the robotic manipulator. The one end of the pendulum-like object was attached to the robot end effector. The other end was either fixed to the environment or attached to the handle of the human interaction partner dependent on the experimental condition. We recorded the interaction forces using JR3 force/torque sensors. For analysis only, a Qualisys motion-capture system recorded the position and orientation of the manipulated objects and of the human handle. Table I lists the pendulum parameters.

2) Software Implementation: The motion capture data was recorded at 200 Hz and the force/torque data at 1 kHz by individual computational units and streamed to a MATLAB/Simulink Real-Time Target model, which was run at 1 kHz. The same model contained the presented energy based controller as well as the low-level velocity controller of the robotic manipulator. The force/torque data[9] at the robot's interaction point were the only input to the energy-based controller. For the analysis, we applied a third-order Butterworth low-pass filter with cutoff frequency 4 Hz to the motion capture data as well as the force/torque data. The filtering circumvented problems arising from numerical differentiation due

[9]The 8-kHz force/torque data were filtered by a first-order low-pass filter with cutoff frequency 500 Hz provided by JR3 before being sampled at 1 kHz.

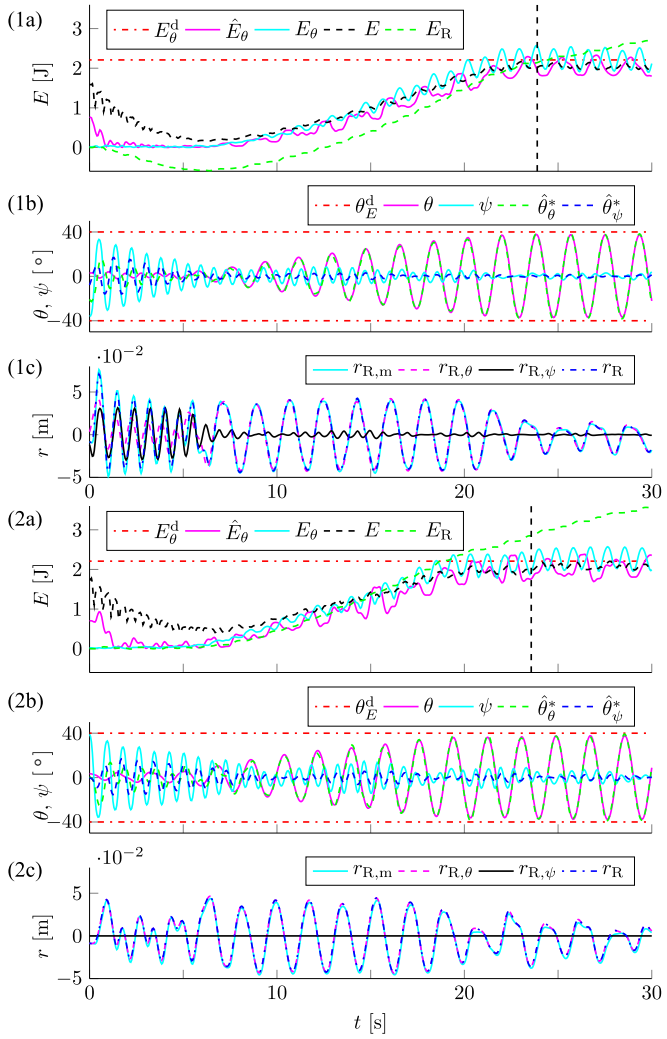

Fig. 5. Experimental results for RL-0 (1a–1c) with ψ-damping and (2a–2c) without ψ-damping. (a) Desired E_θ^{d}, estimated $\hat{E}_\theta$, and actual E_θ energy contained in θ-oscillation, complete pendulum energy E, robot E_{R} energy input. (b) Desired maximum θ_E^{d} deflection angle, extracted projected deflection angles θ_θ^* and θ_ψ^*, and actual deflection angles θ and ψ. (c) Actual robot trajectory $r_{\mathrm{R,m}}$ and commanded robot trajectory $r_{\mathrm{R}} = r_{\mathrm{R},\theta} + r_{\mathrm{R},\psi}$.

to outliers or the undersampling of the motion data with respect to the force/torque data.

3) Controller Parameterization: The controller parameters were tuned in simulation and based on initial experiments (see Table I).

C. Measures

1) Analysis of the Projection onto the Abstract Cart–Pendulum: The projection of the complex pendulum onto the abstract cart–pendulum allows extraction of the dominant oscillation DoFs θ_θ^* and θ_ψ^* and their respective energy levels, $\hat{E}_\theta$ and $\hat{E}_\psi$. The approximations were compared against the actual motion of the pendulum mass m_{p} obtained from the motion capture data, as the actual deflection angles θ and ψ. Based on the actual deflection angle θ, the energy contained in the θ-oscillation E_θ was calculated according to (3). The complete pendulum energy was obtained from the motion capture data of the t-pendulum $E = m_{\mathrm{p}} g y_{\mathrm{p}} + \frac{1}{2} \dot{\boldsymbol{\xi}}_{\mathrm{p}}^T \boldsymbol{M}_{\mathrm{p}} \dot{\boldsymbol{\xi}}_{\mathrm{p}}$, with pendulum mass height y_{p} and pendulum mass velocity $\dot{\boldsymbol{\xi}}_{\mathrm{p}} = \begin{bmatrix} \dot{\boldsymbol{r}}_{\mathrm{p}} & \dot{\boldsymbol{\Omega}}_{\mathrm{p}} \end{bmatrix}$ including translational and rotational velocities, respectively. The 6×6 mass matrix $\boldsymbol{M}_{\mathrm{p}}$ consists of the 3×3 diagonal matrix with the pendulum mass m_{p} as diagonal entries and the 3×3 inertia tensor $\boldsymbol{I}_{\mathrm{p}}$. We approximated the pendulum inertia $\boldsymbol{I}_{\mathrm{p}}$ by a cylinder of length l_{p}, diameter d_{p}, and evenly distributed mass m_{p}. All variables are expressed in the fixed world coordinate system located such that $y_{\mathrm{p}} = 0\,\mathrm{m}$ for $\theta = \psi = 0°$. Under the assumption of two dominant oscillation DoFs and negligible handle velocity, the actual energy contained in the ψ-oscillation is $E_\psi = E - E_\theta$.

2) Analysis of the Controller Performance: To analyze the controller performance, we calculated the settling time T_{s} and the steady-state error e. The settling time T_{s} is the time after which the energy E_θ stays within bounds $\pm\epsilon_\theta$ around the energetic steady-state value $\bar{E}_\theta$. We chose the bounds $\epsilon_{\theta,\mathrm{RL-0}} = 16\%$ and $\epsilon_{\theta,\mathrm{RF-HL}} = 25\%$. The steady-state error is defined as $e = E_\theta^{\mathrm{d}} - \bar{E}_\theta$.

3) Analysis of the Effort Sharing: The energy flows of the human and the robot to the pendulum were calculated based on the interaction point velocities and the measured interaction forces $\dot{E}_i = \dot{\boldsymbol{r}}_i^T \boldsymbol{F}_{i,\mathrm{p}}$ with $i = \mathrm{R}, \mathrm{H}$. The effort sharing between the robot and the human under condition RF-HL was analyzed based on the relative contribution of the robot

$$\gamma_{\mathrm{R}} = \frac{\int_0^T \dot{E}_{\mathrm{R}}\, d\tau}{\int_0^T \dot{E}_{\mathrm{R}} + \dot{E}_{\mathrm{H}}\, d\tau} \tag{19}$$

with fixed $T = 17\,\mathrm{s}$ for comparability (vertical dashed–dotted lines in Fig. 6).

D. Results and Discussion

1) Robot Leader and Fixed End (RL-0): The results of the RL-0 experiment are displayed in Fig. 5 with ψ-damping (1a–1c) and without ψ-damping (2a–2c).

a) Projection onto the abstract cart–pendulum

The experimental trials started with significant initial deflection of the disturbance oscillation $\psi(t=0)_{\psi\mathrm{on}} = 35.9°$ and $\psi(t=0)_{\psi\mathrm{off}} = 38.9°$, but close to zero θ-oscillation. This is in accordance with the complete system energy E and the energy contained in the θ-oscillation E_θ, with the difference being the energy contained in the ψ-oscillation. Due to initialization of the observer with the ψ-dominated initial force measurement, the estimates $\hat{\theta}_\theta^* \approx \theta_\theta^*$ and $\hat{E}_\theta$ were initially off. The estimate $\hat{E}_\theta$ approached the actual energy contained in the θ-oscillation E_θ at around 1 s. The estimated deflection angle $\hat{\theta}_\theta^* \approx \theta_\theta^*$ closely followed the actual deflection angle θ. The results show the practicability of the abstract cart–pendulum projection. The observers separate the nonlinearly coupled oscillation DoFs θ and ψ, and the abstract cart–pendulum-based energies reflect the system energy.

b) Performance

The desired energy level E_θ^{d} was reached after settling times $T_{\mathrm{s},\psi\mathrm{on}} = 23.9\,\mathrm{s}$ and $T_{\mathrm{s},\psi\mathrm{off}} = 23.6\,\mathrm{s}$ (vertical dashed lines in Fig. 5) and tracked with steady-state errors $e_{\psi\mathrm{on}} = -0.41\,\mathrm{mJ}$

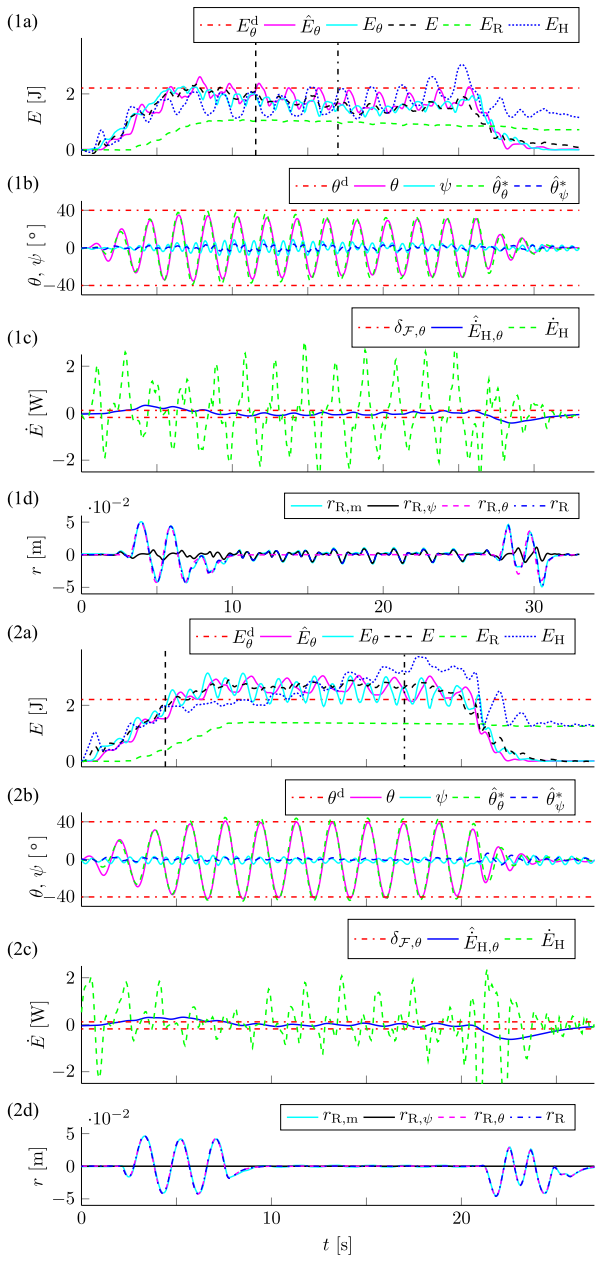

Fig. 6. Experimental results for RF-HL (1a–1d) with ψ-damping and (2a–2d) without ψ-damping. (a) Desired E_θ^{d}, estimated $\hat{E}_\theta$, and actual E_θ energy contained in θ-oscillation, complete pendulum energy E, robot E_{R}, and human E_{H} energy input. (b) Desired maximum θ_E^{d} deflection angle, extracted projected deflection angles θ_θ^* and θ_ψ^*, and actual deflection angles θ and ψ. (c) Follower thresholds $\delta_{\mathrm{u/l},\mathcal{F},\theta}$, estimated $\hat{\dot{E}}_{\mathrm{H},\theta}$, and actual $\dot{E}_{\mathrm{H}}$ human energy flow. (d) Actual robot trajectory $r_{\mathrm{R,m}}$ and commanded robot trajectory $r_{\mathrm{R}} = r_{\mathrm{R},\theta} + r_{\mathrm{R},\psi}$.

and $e_{\psi\mathrm{off}} = -5.98\,\mathrm{mJ}$. With active ψ-damping, the disturbance angle reduced to $|\psi|_{\max,\psi\mathrm{on}} = 7.2^\circ$ within the first 7 s in contrast with $|\psi|_{\max,\psi\mathrm{off}} = 16^\circ$ without active ψ-damping. Close to the energetic steady state, the disturbance oscillation was kept within $|\psi|_{\max,\psi\mathrm{on}} = 3.2^\circ$ and $|\psi|_{\max,\psi\mathrm{off}} = 7.2^\circ$, respectively. The difference between active and inactive ψ-damping is visible in the energy contribution by the robot E_{R}. While the robot hardly influenced the system energy E during the first 6 s without active ψ-damping $E_{\mathrm{R},\psi\mathrm{off}} \approx 0\,\mathrm{J}$, the robot released energy from the ψ-oscillation with active ψ-damping $E_{\mathrm{R},\psi\mathrm{on},\min} = -0.586\,\mathrm{J}$. The active ψ-damping led to a faster decrease of the disturbance oscillation and a smaller remaining disturbance oscillation.[10] This observation confirms the practicability of the approximations made to allow the application of the cart–pendulum swing-up controller to other oscillation DoFs. With respect to controller performance as captured in settling time T_{s} and steady-state error e, no significant difference was observable between the controllers with and without active ψ-damping.[11] Natural damping is shown to be sufficient to keep the disturbance oscillation in relatively small bounds. This result is further supported by the observation that more energy E_{d} dissipated without ψ-damping: $E_{\mathrm{d},\psi\mathrm{off}} > E_{\mathrm{d},\psi\mathrm{on}}$ under conservation of energy $E = E(t=0) + E_{\mathrm{R}} - E_{\mathrm{d}}$. In summary, the control goals for the leader as formulated in (4) are achieved using the presented θ-excitation controller with and without active ψ-damping, but with a lower ϵ_ψ for active ψ-damping.

c) Combination of θ-excitation and ψ-damping

A simple summation combines θ-excitation and ψ-damping to one control input. The actual robot trajectory $r_{\mathrm{R,m}}$ is a combination of θ-excitation at frequency ω_θ, ψ-damping at frequency ω_ψ (if active), and the influence of the joint impedance control of the robot. Even though the oscillation DoFs θ and ψ are nonlinearily coupled, simulations and experiments show that a separate control of the two oscillation DoFs is possible through simple addition. However, the effectiveness of our control approach depends on how similar the individual oscillations are to a simple pendulum oscillation. We conducted additional experiments to examine the limits of our controller with respect to θ_E^{d}. For high energies contained in the θ-oscillation $\theta_E > 60^\circ$, the ψ-oscillation is less simple pendulum-like and the effectiveness of our active ψ-damping diminishes, and active ψ-damping can even have a negative effect on the ψ-oscillation (see [26]).

2) Robot Follower and Human Leader (RF-HL): Fig. 6 displays results under experimental condition RF-HL with ψ-damping (1a–1d) and without ψ-damping (2a–2d).

a) Human interaction partner: The human partner started to inject energy into the t-pendulum at $t = 0\,\mathrm{s}$, which was initially at rest. At $t_{\psi\mathrm{on}} = 2.9\,\mathrm{s}$ and at $t_{\psi\mathrm{off}} = 2.1\,\mathrm{s}$, the estimated energy flow of the human exceeded the threshold $\hat{\dot{E}}_{\mathrm{H},\theta} > \delta_{\mathrm{u},\mathcal{F},\theta}$ and the robot started to inject energy as well. The energetic steady state was reached after settling times $T_{\mathrm{s},\psi\mathrm{on}} = 11.6\,\mathrm{s}$ and $T_{\mathrm{s},\psi\mathrm{off}} = 4.4\,\mathrm{s}$ with steady-state errors $e_{\psi\mathrm{on}} = 664\,\mathrm{mJ}$ and $e_{\psi\mathrm{off}} = -319\,\mathrm{mJ}$. The disturbance oscillation stayed within bounds of $|\psi|_{\max,\psi\mathrm{on}} = 9^\circ$ and $|\psi|_{\max,\psi\mathrm{off}} = 7^\circ$. The performance of the robot follower highly depends on the performance of the human leader. The human's precision was significantly lower compared to the one of the robot, also because the human could only estimate the pendulum energy at the turning points of the pendulum. This explains the higher steady-state errors compared with the RL-0 experiments. Furthermore, the

[10] See videos for a comparison of natural with active ψ-damping in [26].

[11] Note that the initial conditions varied slightly from experimental trial to trial, as the object was hold in the initial configuration by hand. Multiple trials yielded similar results.

experimental results of different trials with a human interaction partner can differ significantly, as, e.g., reflected in the different steady-state errors for the two trials presented. However, throughout all trials, the performance values without active ψ-damping clearly outperformed the performance values with active ψ-damping in contrast to the RL-0 experiments. The feedback of the human interaction partner as well as the recorded data indicate that the active ψ-damping irritates the human interaction partner and, thus, impairs the human's performance. Without active ψ-damping, the robot end effector only slightly oscillated due to the impedance control during the energetic steady state, whereas the robot constantly moved with active ψ-damping.

b) Effort sharing

The relative contribution of the robot with respect to the swing-up was $\gamma_{\mathrm{R},\psi\mathrm{on}} = 0.323$ and $\gamma_{\mathrm{R},\psi\mathrm{off}} = 0.295$. For both controllers, peaks were visible in the actual human energy flow $\dot{E}_{\mathrm{H}}$, which is in accordance with the observations made during human–human rigid object swinging [4]. The projection onto the abstract cart–pendulum as well as the filtering led to a delayed but smooth human energy flow estimate $\hat{\dot{E}}_{\mathrm{H},\theta}$. This estimate stayed within the follower thresholds during the energetic steady state. The energy release of the human was detected by the robot at $t_{\psi\mathrm{on}} = 27.3\,\mathrm{s}$ and $t_{\psi\mathrm{off}} = 21.0\,\mathrm{s}$, and the robot started to move to release energy from the system as well. However, the energy released by the robot was negligible compared with the energy released by the human. The correct detection of the human intention, i.e., goal-directed energy injection and release, further supports the practicability of the abstract cart–pendulum projection. With and without active ψ-damping, the robot took over a significant share of the swing-up task effort. The low effort share of the robot during swing-down was due to natural damping, which helped the human interaction partner to achieve especially fast energy release. Note that we adjusted the lower follower threshold $\delta_{\mathrm{l},\mathcal{F},\theta}$ such that natural damping is not interpreted as energy release initiated by the human partner. In summary, we were able to achieve the control goal for the follower of identifying and imitating the energy flow of the leader as formulated in (5).

3) Maximum Energy Content θ_E^d: We limited the desired energies to $\theta_E^{\mathrm{d}} = 40^\circ$ for the RL-0 condition, because the fixed end caused increased ψ-oscillations for high θ_E[12] and for the RF-HL condition, in order to enable the human leader to sustain a steady-state oscillation for comparability, which gets more difficult with higher θ_E. In order to find the limits of our controller, we performed additional experiments with a robot leader and a passive human, i.e., the human partner allowed his hand to passively move with the swinging pendulum. Our results show that the controller can reach $\theta_E^{\mathrm{d}} = 70^\circ$. However, we had to restrict the amplitude factor to $\bar{a} = 0.12\,\mathrm{m}$ due to joint velocity limitations. As a consequence, the controller saturated and was not able to reach the desired energy levels $\theta_E^{\mathrm{d}} = 80$ and 90° (see [26]). An energy content of $\theta_E^{\mathrm{d}} = 70^\circ$ for our pendulum of $l^* = 0.77\,\mathrm{m}$ would, e.g., allow the object to reach a height $h_E = 0.47\,\mathrm{m}$ at a distance $x = 0.77\,\mathrm{m}$ from the pivot point after being released at $\theta = 60^\circ$. Robot manipulator motion for a controlled landing at an elevated location as motivated in Fig. 1 could be realized, e.g., by similar methods as presented in [3] and will be part of our future work.

[12]This was also the case for HL-0.

V. Conclusion

In this paper, we have presented a control approach for two-agent cooperative swinging of complex pendulum-like objects. We show experimentally that our approach of projecting the complex pendulum-like object onto an abstract cart–pendulum allows us to separate desired and undesired oscillation DoFs. We regulate the energies of the individual oscillation DoFs through the application of a cart–pendulum swing-up controller. Therefore, the effectiveness of our control approach depends on how simple pendulum-like the individual oscillations are. The simple pendulum-like desired oscillation DoF of the complex pendulum is excited such that a desired energy level is reached. The less simple pendulum-like undesired oscillation can be simultaneously damped for moderate energy levels of the desired oscillation through summation of two control inputs. The experiments did not reveal clear benefit of active disturbance damping, but natural damping seemed to be sufficient. Experiments with a human interaction partner indicate further that active disturbance damping irritates the human partner. We realize robotic follower behavior through imitation of the energy flow produced by the leading partner. This energy flow is solely estimated from the measured interaction force and relies on the abstract cart–pendulum projection. Experiments showed that the robotic follower can take over a substantial share of the swing-up effort to a desired energy level, which is only known to the leading human partner.

We are currently extending the presented approach to adaptive control, such that dimensions and mass do not have to be known in advance. In a next step, we plan to combine the results from pendulum-like object swinging with our findings from rigid object swinging in order to enable cooperative swinging of bulky flexible objects for controlled placing of these objects at elevated locations.

Acknowledgment

The authors would like to thank S. Hirche for laboratory space and equipment; F. Wirnshofer and J. Lu for their help with the experiments; and F. Christange, L. Alkurdi, Dr. M. Leibold, M. Schill, M. Semmler, and S. Kersting for their valuable advice.

References

[1] M. Bernard and K. Kondak, "Generic slung load transportation system using small size helicopters," in *Proc. IEEE Int. Conf. Robot. Autom.*, 2009, pp. 3258–3264.

[2] M. T. Mason and K. Lynch, "Dynamic manipulation," in *Proc. IEEE/RSJ Int. Conf. Intell. Robots Syst.*, Jul. 1993, vol. 1, pp. 152–159.

[3] D. Cunningham and H. Asada, "The Winch-Bot: A cable-suspended, under-actuated robot utilizing parametric self-excitation," in *Proc. IEEE Int. Conf. Robot. Autom.*, May 2009, pp. 1844–1850.

[4] P. Donner, F. Wirnshofer, and M. Buss, "Controller synthesis for human-robot cooperative swinging of rigid objects based on human-human experiments," in *Proc. 23rd IEEE Int. Symp. Robot Human Interactive Commun.*, Aug. 2014, pp. 586–592.

[5] D. Zameroski, G. Starr, J. Wood, and R. Lumia, "Rapid swing-free transport of nonlinear payloads using dynamic programming," *J. Dyn. Syst., Meas. Control*, vol. 130, no. 4, pp. 041001-1–041001-11, 2008.
[6] C. de Crousaz, F. Farshidian, M. Neunert, and J. Buchli, "Unified motion control for dynamic quadrotor maneuvers demonstrated on slung load and rotor failure tasks," in *Proc. IEEE Int. Conf. Robot. Autom.*, Seattle, WA, USA, 2015, pp. 2223–2229.
[7] S. Lefrancois and C. Gosselin, "Point-to-point motion control of a pendulum-like 3-DOF underactuated cable-driven robot," in *Proc. IEEE Int. Conf. Robot. Autom.*, May 2010, pp. 5187–5193.
[8] D. Zanotto, G. Rosati, and S. Agrawal, "Modeling and control of a 3-DOF pendulum-like manipulator," in *Proc. IEEE Int. Conf. Robot. Autom.*, May 2011, pp. 3964–3969.
[9] N. Zoso and C. Gosselin, "Point-to-point motion planning of a parallel 3-DOF underactuated cable-suspended robot," in *Proc. IEEE Int. Conf. Robot. Autom.*, May 2012, pp. 2325–2330.
[10] C. Gosselin and S. Foucault, "Dynamic point-to-point trajectory planning of a two-DOF cable-suspended parallel robot," *IEEE Trans. Robot.*, vol. 30, no. 3, pp. 728–736, Jun. 2014.
[11] Y. Maeda, A. Takahashi, T. Hara, and T. Arai, "Human-robot cooperation with mechanical interaction based on rhythm entrainment-realization of cooperative rope turning," in *Proc. IEEE Int. Conf. Robot. Autom.*, 2001, vol. 4, pp. 3477–3482.
[12] C. H. Kim, K. Yonekura, H. Tsujino, and S. Sugano, "Physical control of the rotation center of an unsupported object rope turning by a humanoid robot," in *Proc. 9th IEEE-RAS Int. Conf. Humanoid Robots*, Dec. 2009, pp. 148–153.
[13] K. Kosuge, H. Yoshida, and T. Fukuda, "Dynamic control for robot-human collaboration," in *Proc. 2nd IEEE Int. Workshop Robot Human Commun.*, Nov. 1993, pp. 398–401.
[14] B. Corteville, E. Aertbelien, H. Bruyninckx, J. De Schutter, and H. Van Brussel, "Human-inspired robot assistant for fast point-to-point movements," in *Proc. IEEE Int. Conf. Robot. Autom.*, Apr. 2007, pp. 3639–3644.
[15] K. Reed, M. Peshkin, M. Hartmann, J. Patton, P. Vishton, and M. Grabowecky, "Haptic cooperation between people, and between people and machines," in *Proc. IEEE/RSJ Int. Conf. Intell. Robots Syst.*, Oct. 2006, pp. 2109–2114.
[16] P. Evrard and A. Kheddar, "Homotopy switching model for dyad haptic interaction in physical collaborative tasks," in *Proc. WHC EuroHaptics*, Mar. 2009, pp. 45–50.
[17] A. Mörtl, M. Lawitzky, A. Kucukyilmaz, M. Sezgin, C. Basdogan, and S. Hirche, "The role of roles: Physical cooperation between humans and robots," *Int. J. Robot. Res.*, vol. 31, no. 13, pp. 1656–1674, 2012.
[18] V. Fernandez, C. Balaguer, D. Blanco, and M. Salichs, "Active human-mobile manipulator cooperation through intention recognition," in *Proc. IEEE Int. Conf. Robot. Autom.*, 2001, vol. 3, pp. 2668–2673.
[19] S. Kajita, F. Kanehiro, K. Kaneko, K. Yokoi, and H. Hirukawa, "The 3D linear inverted pendulum mode: A simple modeling for a biped walking pattern generation," in *Proc. IEEE/RSJ Int. Conf. Intell. Robots Syst.*, 2001, vol. 1, pp. 239–246.
[20] J. Nakanishi, T. Fukuda, and D. Koditschek, "A brachiating robot controller," *IEEE Trans. Robot. Autom.*, vol. 16, no. 2, pp. 109–123, Apr. 2000.
[21] K. Åström and K. Furuta, "Swinging up a pendulum by energy control," *Automatica*, vol. 36, no. 2, pp. 287–295, 2000.
[22] M. Spong, "The swing up control problem for the acrobot," *IEEE Control Syst.*, vol. 15, no. 1, pp. 49–55, Feb. 1995.
[23] K. Yoshida, "Swing-up control of an inverted pendulum by energy-based methods," in *Proc. Amer. Control Conf.*, vol. 6, 1999, pp. 4045–4047.
[24] P. Donner, A. Mörtl, S. Hirche, and M. Buss, "Human-robot cooperative object swinging," in *Proc. IEEE Int. Conf. Robot. Autom.*, May 2013, pp. 4343–4349.
[25] P. Donner, F. Christange, and M. Buss, "Human-robot cooperative swinging of complex pendulum-like objects," in *Proc. IEEE/RSJ Int. Conf. Intell. Robots Syst.*, Nov. 2013, pp. 4602–4608.
[26] Additional videos of t-pendulum experiments. [Online]. Available: https://www.lsr.ei.tum.de/videos/. Accessed on: April 26, 2016.
[27] L. S. Cicolani and G. Kanning, *Equations of Motion of Slung-Load Systems, Including Multilift Systems*, vol. 3280. National Aeronautics and Space Administration, Office of Management, Scientific and Technical Information Program, 1992.